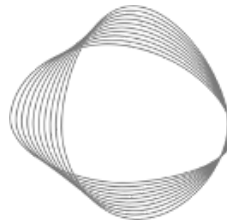


# Agriculture - Cropland Biomass Fires Emissions Methodology

Ishaan Kochhar, Saheel Ahmed, and Amber Luong

All authors affiliated with Blue Sky Analytics



CLIMATE  
TRACE

## 1. Introduction

Open burning of biomass - whether from wildfires or anthropogenic sources, such as the burning of crop residues - is one of the sources of greenhouse gas (GHG) emissions and air quality hazards such as particulate pollution (Jacobson, 2014). There are many reasons to burn agricultural land, including to clear residue, fertilize the soil, and eliminate pests and weeds, and it is often deeply rooted in culture (Korontzi et al., 2006). During the crop season of clearing fields and planting new ones, farmers burn remnants of old crops to rid them of grasses and scrub. Additionally, this action replenishes nutrients in the soil, which help to ensure a healthy crop the following season.

The burning of agricultural, cropland, or managed land is not confined to developing countries. In countries where the practice is controlled or restricted, it contributes to regional air quality and national emissions (U.S. Environmental Protection Agency, 2021). Cropland burning will likely continue contributing to global trace gas and particulate emissions due to the increasing human population and changing land use practices that allow agricultural expansion and intensification (Korontzi et al., 2006).

Biomass fires are a source of three major GHGs: carbon dioxide ( $\text{CO}_2$ ), methane ( $\text{CH}_4$ ), and nitrous oxide ( $\text{N}_2\text{O}$ ). Estimating the emissions associated with biomass fires requires a few fundamental inputs which are analogous to the inputs used in many emissions calculations: fuel type (i.e., vegetation type), the quantity of fuel burned, and emissions factors specific to each fuel type and GHG to be estimated. However, since fires are dynamic and move, variables such as the quantity of fuel burned need to be reassessed for each area of interest and time, or ideally, for each fire occurrence. Seiler and Crutzen (1980) introduced a method for estimating biomass fire emissions using the following relationship (Eq. 1.).

$$\text{Emissions (g)} = \text{BA(ha)} * \text{BFL (kg/ha)} * \text{FFC (\%)} * \text{EF(g/kg)} \quad (\text{Eq. 1})$$

where,  $\text{BA}$  = Burned Area,  $\text{BFL}$  = Biomass Fuel Load,  $\text{FFC}$  = Fraction of Fuel Consumed, and  $\text{EF}$  = Emission Factor.  $\text{Emissions}$  in Eq.1 represents total estimated trace gas emissions in grams, the quantity of fuel burned is determined by the product of the fuel load (amount of biomass available per hectare) and the fraction of fuel consumed (i.e., combustion completeness). This method can still be used for smaller-scale inventories where ground-level data collection is feasible.

## Satellite-based emissions estimation methods

The advent of satellite data sources for detecting burned areas and active fires enabled the development of global-scale fire emissions inventories. These remote sensing-based inventories can be broadly categorized into two approaches, bottom-up and top-down, although in practice, some inventories combine elements of both.

Several dedicated fire emissions inventories exist, including Global Fire Emissions Database (GFED) (Van der Werf et al., 2017, 2010), the Global Fire Assimilation System (GFAS) (Kaiser et al., 2012), and the Fire Energetics and Emissions Research (FEER) (Ichoku and Ellison, 2014; Ichoku and Kaufman, 2005), but their usage is more common in the scientific community than in the policy community.

Bottom-up inventories have used the Seiler and Crutzen (1980) approach with satellite data to estimate the biomass fuel quantity burned using detections of the burned area along with other observed and modeled factors. For example, the Global Fire Emissions Database (GFED) combines satellite observations of burned areas, active fires, and plant productivity to generate emissions estimates (Randerson et al., 2017; Van der Werf et al., 2010). However, several challenges exist in applying bottom-up methods. Some sources have cited a tendency to underestimate emissions in regions dominated by smaller fires and the inherent uncertainty in measurements of vegetation quantity and combustion completeness (Kasischke et al., 2011; Ramo et al., 2021). In addition, the focus on burned areas means that fire activity can only be detected days to weeks after the actual fire occurrence, which does not allow for applications requiring near real-time estimates.

Top-down inventories, rather than bottom-up (e.g., GFED), use satellite observations of fire radiative power (FRP) as the basis for estimating emissions. FRP is the emitted radiative energy (in units of power, such as megawatts MW) by a fire at the time of observation. An example of a top-down inventory is the Global Fire Assimilation System (GFAS), which provides daily estimates of the emissions flux (in  $\text{kg m}^{-2} \text{s}^{-1}$ ) for a wide range of pollutants and GHGs from fires (Kaiser et al., 2012). The primary advantage of the top-down approach over the bottom-up is the near-real-time aspect, which can generate global near-real-time (within days) emissions estimates. It also eliminates the need for the difficulty in calculating combustion completeness and fuel load using small-scale manual lab experiments with a more generalized statistical and remote sensing-based approach using aerosol optical depth (AOD) and fire radiative power (FRP).

Other top-down approaches are based on fire radiative energy (FRE), the time integral of FRP. Controlled lab experiments have shown a linear relationship between FRE and biomass combustion rate. Studies have applied this approach to estimate biomass combustion using the product of FRE and a combustion coefficient (Freeborn et al., 2008; Hudak et al., 2016; Wooster et al., 2005). These approaches yield the following equation to estimate emissions (Eq. 2):

$$Emissions = \int_0^{24} FRP(MW)dt * Combustion\ Coefficient(g/MJ) * EF(g/kg) \quad (Eq.\ 2)$$

Where *Emissions* are the total estimated emissions for a trace gas in milligrams from biomass burning, *FRP* represents the fire radiative power measurement of individual active fire pixels in megawatts (MW) integrating over 24 hour period to fire radiative energy (FRE) in megajoules (MJ), *Combustion Coefficient* is vegetation specific measurements in g/MJ derived by the linear correlation between total particulate matter TPM (g) and time integral FRP (MJ), *EF* emissions factors representative of the biome & trace gas specific measurements.

The present study provides a global assessment of fire activity in established agricultural lands and aims to identify regional patterns in agricultural burning from 2015 to 2020 using the top-down approach. The top-down approach from Eq. 2 was selected to estimate cropland biomass fire emissions.

## 2. Materials and Methods

This section looks at the top-down approach we applied to estimate emissions from global biomass fires from croplands. The core methodology remains the same for both country-level and asset-level estimates since the top-down approach begins with individual fire detections and their characteristics, provided at a 375m spatial resolution and daily frequency from NASA Fire Information for Resource Management (FIRMS). Note that while we use the term “fire detection” for simplicity, technically, a given 375m x 375m pixel area could contain multiple smaller fires. Each fire detection has unique attributes used in the emissions equation, including the fire radiative power (FRP) and biomass/vegetation type.

Since fires, with their lack of spatio-temporal persistence, do not fit the conventional definition of an asset, we needed to define what fire asset-level means for the Climate TRACE inventory. For most sectors, asset-level implies providing emissions for the most granular unit possible to attribute to each point source (e.g., individual ships, power plants, factories). Since the primary goal was the attribution of these emissions, and fires occur across a range of land types - wild/unmanaged areas, managed lands, public ownership, and private ownership - the most consistent way to attain a level of attribution across all fire types was to use a highly granular self-defined regular geographic grid. Therefore, for this purpose, asset-level fire data was provided as the sum of all emissions for cropland aggregated at the spatial resolution of 0.25 degrees (~25km spatial resolution) across all countries.

### 2.1 Datasets employed

#### 2.1.1 Remote sensing datasets

Multiple remote sensing datasets were employed to derive biomass fire emissions. Table 1 summarizes each dataset with detailed descriptions in the text.

**Table 1** Remote sensing and derived data sets employed.

Satellite (Sensor)	Bands or Datasets	Purpose	Temporal; Spatial Resolution; Coverage
Suomi NPP (VIIRS) Active Fire Dataset VNP14IMGTDL_NRT	Derived from I-band	Identify active fires and Fire Radiative Power (FRP)	Daily; 375m; Global
Aqua and Terra (MODIS) Thermal Anomalies/Fire Daily L3 Aqua (MYD14A1) Terra (MOD14A1)	MaxFRP	Derive combustion coefficients	Daily; 1 km Global
Aqua and Terra (MODIS) MAIAC AOD MCD19A2	Optical Depth 055	Derive combustion coefficients	Daily; 1 km; Global
Copernicus Global Land Cover CGLS-LC100 collection	Derived dataset	Land cover classification	Annual; 100m; Global

### **Suomi NPP (VIIRS) Active Fire Dataset**

The Visible Infrared Imaging Radiometer Suite (VIIRS) aboard the Suomi National Polar-orbiting Partnership (NPP) satellite provides the active fire data (Giglio and Justice, 2015) and was used as a primary input in estimating biomass fire emissions. The dataset was acquired from the NASA FIRMS website. The dataset provided information about the locations and the Fire Radiative Power (FRP) at a spatial resolution of 375m daily. This source was selected specifically for its ability to detect smaller fires and improved night-time performance (compared to other commonly used active fire products with 1 km resolution). The 3040 km VIIRS swath enables ~15% image overlap between consecutive orbits at the equator, providing complete global coverage every 12 hours. Suomi NPP has nominal (equator crossing) observation times at 1:30 p.m. and 1:30 a.m. Mean Local Time (MLT).

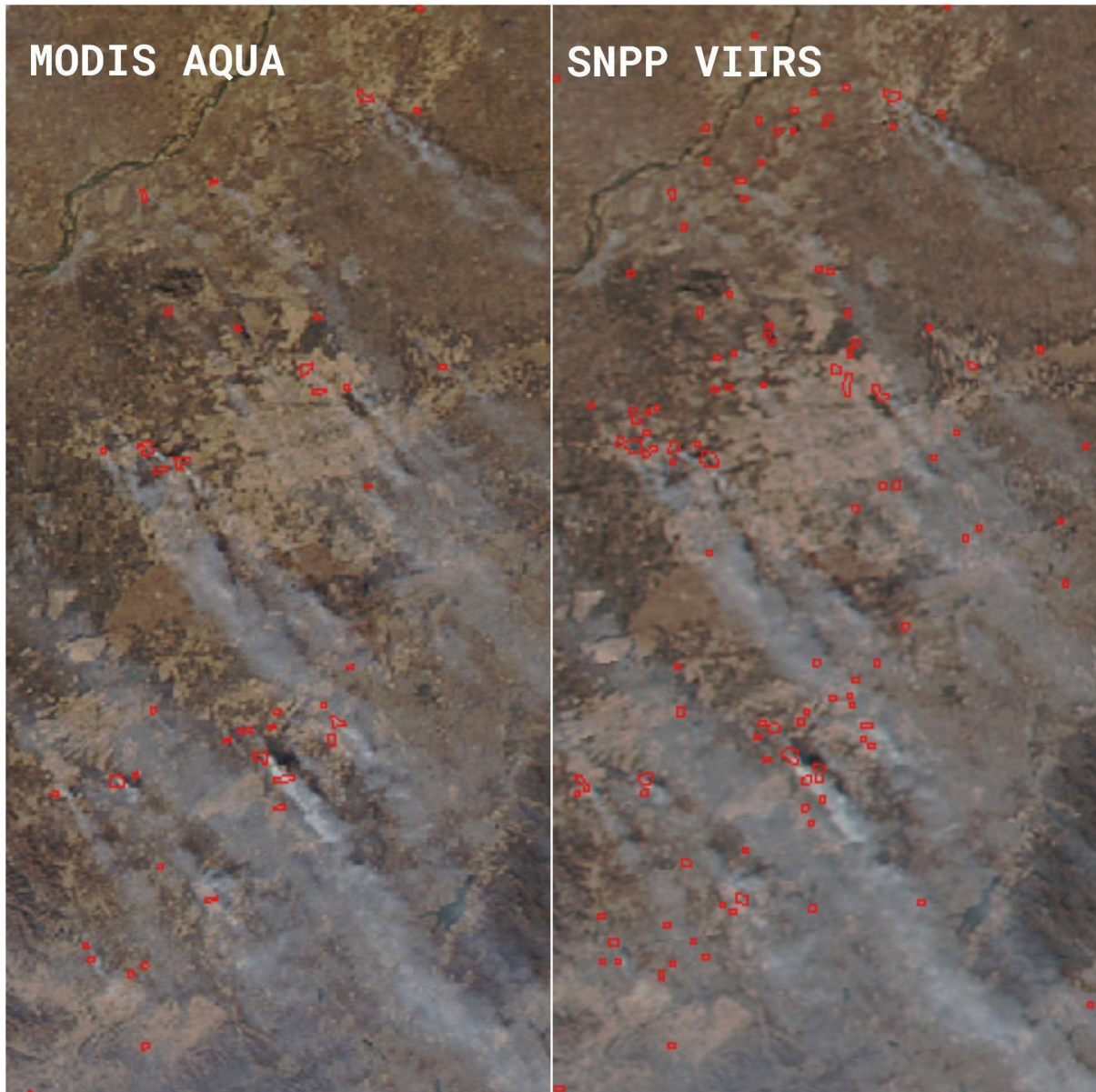


**Figure 1** (Left) MODIS Aqua detected fire hotspots from managed land, and (right) VIIRS Suomi NPP detected fire hotspots from managed land on 6 Nov 2016 in China.

#### Thermal Anomalies/Daily Fire L3 Aqua (MYD14A1) and Terra (MOD14A1)

To perform the aerosol and fire pixel level matching at a close spatial and temporal proximity, FRP data was acquired from the same Terra and Aqua at 1 km spatial resolution. The Aqua Moderate Resolution Imaging Spectroradiometer (MODIS) instrument acquires data twice daily (10:30 a.m. and p.m.), as does the Terra MODIS (1:30 p.m. and a.m.). The MOD14A1 (Terra) and MYD14A1 (Aqua) Collection 6 (Giglio and Justice, 2015) used are produced every 8 days at 1 km spatial resolution. The dataset consists of a fire mask (FireMask), pixel quality indicators (QA), and maximum fire radiative power (MaxFRP) for each day in the 8 days packaged into a single file.

While FRP data from S-NPP and MODIS were used in the model deployment, only S-NPP was used for the daily fire detections. MODIS data (FRP and AOD) were used solely to

derive the updated combustion coefficients as an input to the GHG emissions equation.

### Aerosol Optical Depth

The aerosol optical depth (AOD) product used in this study was acquired from Terra and Aqua combined MODIS Multi-Angle Implementation of Atmospheric Correction (MAIAC) 550 nm at a spatial resolution of 1 km (Lyapustin et al., 2018) (Lyapustin et al., 2011). Due to explicit surface characterization, MAIAC provides a global dataset that provides information on aerosol levels detected from high smoke plume areas. The aerosol optical depth band at 550 nm was retrieved for this application.

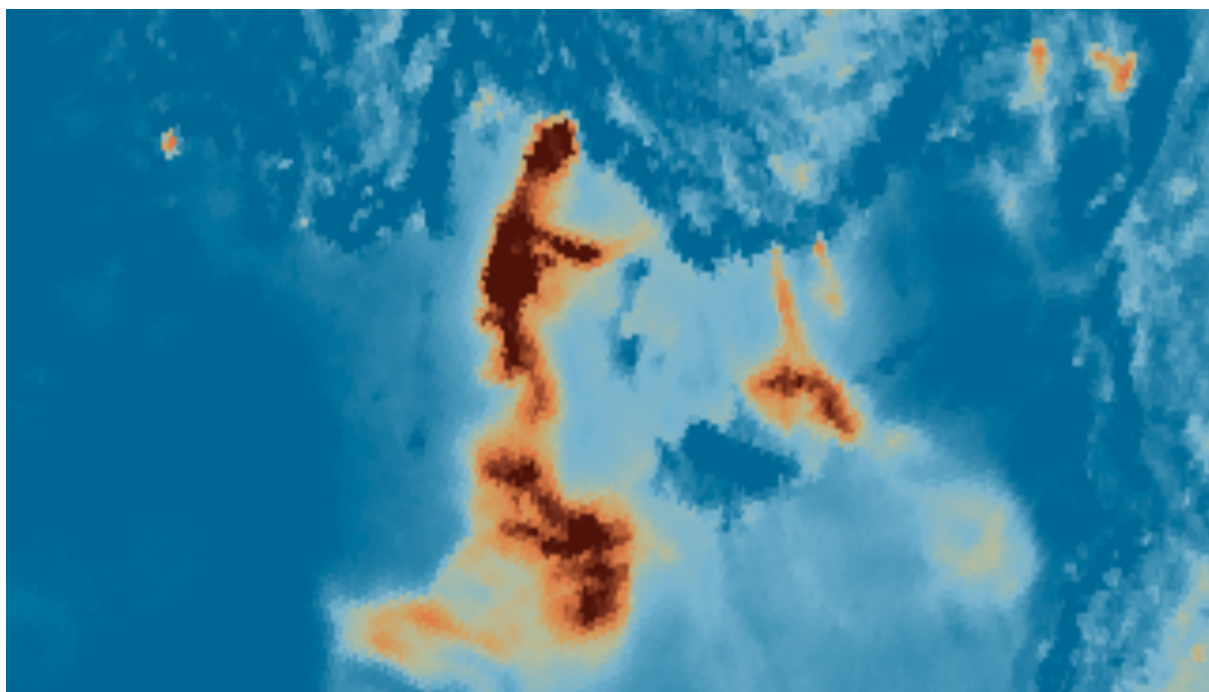


**Figure 2** Aerosol Smoke Plume originating from Antalya, Mersin, Turkey in July 2021, as captured by NASA MODIS-Terra.

### Copernicus Global Land Cover CGLS-LC100 collection

In order to accurately perform vegetation classification for all global fire events, a 100 m global landcover map (collection 3) was acquired from Copernicus Global Land Service (Buchhorn et al., 2020). Global Land Service (CGLS) is part of the Land Monitoring Core Service (LMCS) of Copernicus, the European flagship Earth Observation program. As part of the Global Land Service, a series of bio-geophysical products are produced systematically on the changing global land surface, including global land surface status and land surface evolution. The annual global landcover maps from 2015 to 2019 were accessed and downloaded from the Vito Landcover Viewer (<https://lcviewer.vito.be/download>). The dataset consists of 23 land cover classes, out of which we selected the managed land class or the cropland class. The dataset has been validated against an independent validation dataset containing approximately 21k points generated in collaboration with regional experts. Validation assessments show high accuracy of 80.3-80.5 for yearly 2016-2019 maps, around 80% at the continental level with the highest accuracy of 83.7% for Asia and the lowest of

77.6% for North America (Buchhorn et al., 2020). The Copernicus land cover dataset was selected as it was the highest-resolution global dataset available for land cover at the time of model deployment. For years 2020 and 2021, which lack a land cover map, the 2019 land cover map was assigned to each year to estimate emissions.

## 2.2 Model

For the current study, top-down model deployment was selected and used as a reference to estimate emissions from anthropogenic biomass-burning events associated with agricultural crop residue. The GHG emissions estimated include carbon dioxide ( $\text{CO}_2$ ), methane ( $\text{CH}_4$ ), and nitrous oxide ( $\text{N}_2\text{O}$ ). The top-down emissions model used was primarily a satellite-based approach. The model was a hybrid of statistical and empirical-based methodology since combustion coefficients, one of the core inputs, was statistically derived using regression analysis on aerosol optical depth (AOD) and fire radiative power (FRP). In this case, the coefficients are calculated by matching coincident pixels for the AOD and the FRP for the cropland land cover class. The final GHG emissions were estimated using empirical equations.

As described in the previous section, the top-down model inputs include the S-NPP VIIRS, Aqua, and Terra MODIS sensors and the Copernicus 100m land cover map (Figure 7). The model generated emissions estimates for cropland in the native resolution of active fire data (375 m), which were then aggregated using a regular grid of 0.25 degrees. Furthermore, all GHGs were combined into  $\text{CO}_2\text{eq}$  20 and  $\text{CO}_2\text{eq}$  100-year global warming potential (GWP) from the IPCC 6th assessment report (Forster et al., 2021).

## 2.3 Methods



**Figure 3** Top-Down Methodology to estimate biomass GHG emissions.

Definitions of key parameters are described in the section below:

### Key Definitions:

- **Aerosol Optical Depth (AOD)** is the dimensionless measure of aerosols (e.g., smoke particles, dust, sea salt, etc.) distributed within a column of air from a location on the Earth's surface to the top of the atmosphere. Since particles can either absorb or scatter light, AOD is a measure of how much sunlight is blocked from reaching the surface by these particles in a given column of air (Xun et al., 2021).
- **Fire Radiative Energy (FRE)** is the measure of total radiative energy over the lifetime of a fire (in units of energy, such as MWh or MJ), obtained by integrating FRP over a fire's assumed duration (Vermote et al., 2009).

- **Fire Radiative Power (FRP)** is the rate of emitted radiative energy (in units of power, such as MW) by a fire at the time of observation (Vermote et al., 2009).
- **Total Particulate Matter (TPM)** is the measure (in units of mass, such as g) of the mixture of solid particles and liquid droplets found in the air, including microscopic and visible particles.

The workflow to estimate the GHG emissions is provided above and highlighted in Figure 3:

1. The data cleaning and quality check process involved:
  - a. Filtering to exclude fires with a confidence level less than 50 percent (a self-defined threshold choice), as low confidence daytime fires are often false detections associated with sunglint and other temperature anomalies.
  - b. Filtering only to include fires labelled type 0 (vegetation fires), removing other types associated with volcanic eruptions, gas flares, etc.
2. To calculate total emissions, the FRP for each fire detection needs to be converted into FRE, which is the time integral of FRP (in MJ), as described by the relationship in Eq. 3. The diurnal cycle width is an approximation of how long a fire persists (in hours; Figure 4). This duration will vary based on factors such as the biomass fuel type, region, and weather conditions (Eq. 4).

$$FRE = \int_0^{24} FRP dt \text{ (Eq. 3)}$$

$$FRE = FRP * \Delta Diurnal Cycle Width \text{ (Eq. 4)}$$

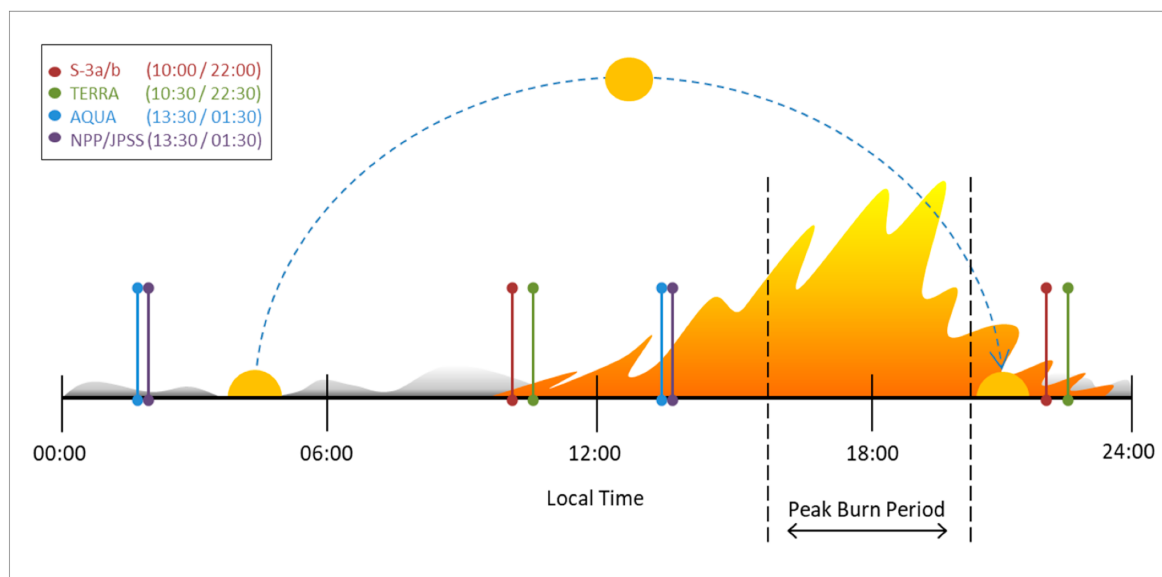


**Figure 4** The nature of the diurnal cycle of fire with the peak period around 6 pm overlapping with the overpass time of polar satellites - Aqua, Terra, SNPP, S3. Source Johnston et al. (2020).

3. Since we use S-NPP, a polar-orbiting satellite, as the source for identifying fire locations (as illustrated in Figure 4), only a very limited portion of the fire diurnal cycle is captured because the polar orbit means that the satellite will only capture two observations of a given location in a 24-hour period). We, therefore, incorporate assumptions for the diurnal cycle width for each of our defined land cover classes based on earlier fire observation studies using geostationary satellites (Andela et al., 2015). These satellites provide a complete understanding of the full diurnal cycle by observing a given location every 15 minutes.
  
4. We selected the cropland class from the Copernicus Global Land Cover CGLS-LC100 collection 3 (Buchhorn et al., 2020)
  - a. We first omitted any non-vegetation-specific land cover classes from the 23 total classes (e.g., built environment, water, snow).
  - b. Additionally, omitted any vegetation class not defined as cropland class.
  - c. For each fire detection, we assigned the cropland class by taking a majority class within the grid cell of size 375m \* 375 m class.
  
5. We derived the combustion coefficient for cropland GHG with a satellite-based methodology that uses properties of observed fires in that land cover class (FRP, AOD, TPM). It uses a fire matchup technique to correlate total particulate matter (TPM) calculated from AOD with fire radiative energy (FRE) calculated from time-integrated FRP. This methodology is based on a number of studies from the literature (Mota and Wooster, 2018; Ichoku and Ellison, 2014; Ichoku and Kaufman, 2005; Wooster et al., 2005).
  
6. We obtained the emission factors for CO<sub>2</sub>, CH<sub>4</sub>, and N<sub>2</sub>O corresponding to cropland class, based on (Andreae, 2019) (the most recent update from the same author referenced in the IPCC 2006 guidelines).

**Table 2** Emissions factor adapted from Andreae (2019) and Andreae and Merlet (2001). Units are in g/kg.

Trace Gas	Emission factor managed Lands (Croplands)
CO <sub>2</sub>	1440
N <sub>2</sub> O	0.10
CH <sub>4</sub>	5.70

7. The following empirical relationship was used to estimate emissions of each GHG (in tonnes; Eq. 5):

$$GHG\ Emissions\ (t_{GHG(i)}) = FRE * C_{e_{GHG(i)}} * EF_{GHG(i)} * 10^{-9} \ (Eq.\ 5)$$

- FRE is the time integral of FRP in MJ.

- $C_{e_{GHG}}$  is the cropland and GHG dependent combustion coefficient in gMJ<sup>-1</sup>.
  - $E_{GHG}$  is the relevant emissions factor for cropland and GHG in g/kg biomass.
  - $10^{-9}$  (to convert milligrams to tonnes).
  - $t_{GHG(i)}$  GHG (i) emissions for CO<sub>2</sub>, CH<sub>4</sub>, and N<sub>2</sub>O (in tonnes).
8. The resulting CO<sub>2</sub>, CH<sub>4</sub>, and N<sub>2</sub>O estimates were then converted into CO<sub>2</sub> equivalent totals based on the 20-year (GWP<sub>20</sub>; Eq. 6) and 100 years (GWP<sub>100</sub>; Eq. 7) Global Warming Potential values from the IPCC 6th Assessment Report (Forster et al., 2021).
- $$CO_2 \text{ Eqv. Emiss. } (tCO_2 eq)(GWP_{20}) = tCO_2 + (81.2 * tCH_4) + (273 * tN_2O) \text{ (Eq. 6)}$$
- $$CO_2 \text{ Eqv. Emiss. } (tCO_2 eq)(GWP_{100}) = tCO_2 + (27.9 * tCH_4) + (273 * tN_2O) \text{ (Eq. 7)}$$
9. The individual fire detection emissions were then aggregated, across the relevant spatial and temporal resolutions. For Climate TRACE, this aggregation was performed at the 0.25-degree spatial resolution, by the province in each country, and at the country level.

## 2.4 Verifying modeled emissions estimates

Due to the nature of the sector - Forestry & Land Use, it is relatively harder to find an actual source of truth to validate our estimates even at the regional scale. The closest form of ground truth available are existing independent studies done on the same sector and topic at both global and regional scale that allows us to validate our results. To validate our estimated emissions, we had two broad options i) Compare our estimates against emissions inventories from UNFCCC and ii) Compare our estimates against independent studies or global fire emissions inventories based on a similar methodology.

Currently, the Climate TRACE fire sector estimates emissions from croplands. The challenge with validating our estimates with UNFCCC is that it does not report fire emissions as a separate category - they are included in the total Land Use, Land Use-Change, and Forestry (LULUCF) category. LULUCF emissions are reported net, while the current study estimates only reflect gross emissions. UNFCCC national submissions only require reports of fires that are deemed anthropogenic (on managed lands), so their emissions estimates would only represent a fraction of the fires our model captured.

Moving forward from the national inventories and more towards sector-based emissions inventories, for numerical inventory comparisons, we focussed on the two major global emissions inventories which are most closely aligned with the coverage of our model and most readily comparable - Global Fire Emissions Database (GFED) (Van der Werf et al., 2006) and Global Fire Assimilation System (GFAS) (Kaiser et al., 2012). GFED, primarily based on a bottom-up approach, estimates emissions at 0.25 degrees, while GFAS based on a

top-down approach, estimates emissions at 0.125 degrees. Both inventories generate global emissions for various greenhouse gasses; however, they are not entirely independent because GFAS uses combustion coefficients derived from FRP and DMC (dry matter combustion) from GFED, hence sharing the same uncertainties. For the current study, we accessed and downloaded the latest version of both the inventories -

GFED v4.1s were downloaded from: <https://www.geo.vu.nl/~gwerf/GFED/GFED4/>. The datasets were available as HDF files containing carbon emissions ( $gCm^{-2}month^{-1}$ ), dry matter emissions ( $kgDMm^{-2}month^{-1}$ ) and fractional contribution of different fire types. The dataset also included a [python script](#) by Wolfgang Knorr to convert carbon emissions per pixel per month into total CO<sub>2</sub> emissions. Emissions from the current study were aggregated to the 0.25 grid size same as GFED for validation. Time series analysis and correlations were performed from 2015 to 2020 (data from 2021 was added later). Similar analyses were performed for each of the countries around the world with a major emissions footprint.

GFAS v1.2 were downloaded from the ECMWF GFAS ADS website using their API: <https://ads.atmosphere.copernicus.eu/cdsapp#!/dataset/cams-global-fire-emissions-gfas?tab=form>. The datasets were available as NetCDF files containing carbon dioxide emissions flux ( $kgm^{-2}s^{-1}$ ) at 0.125 degrees grid size. The emissions flux was converted into total emissions by multiplying the area of the grid cell and the number of seconds per day as suggested by the ECMWF support team upon inquiry. Similar time series analyses and correlations were performed for the period of 2015 to 2020 at the country level to determine meaningful insights.

Some of the key differences between the current study and the validation sources selected are described in Table 3. The inventories were chosen because they are widely used and easily accessible.

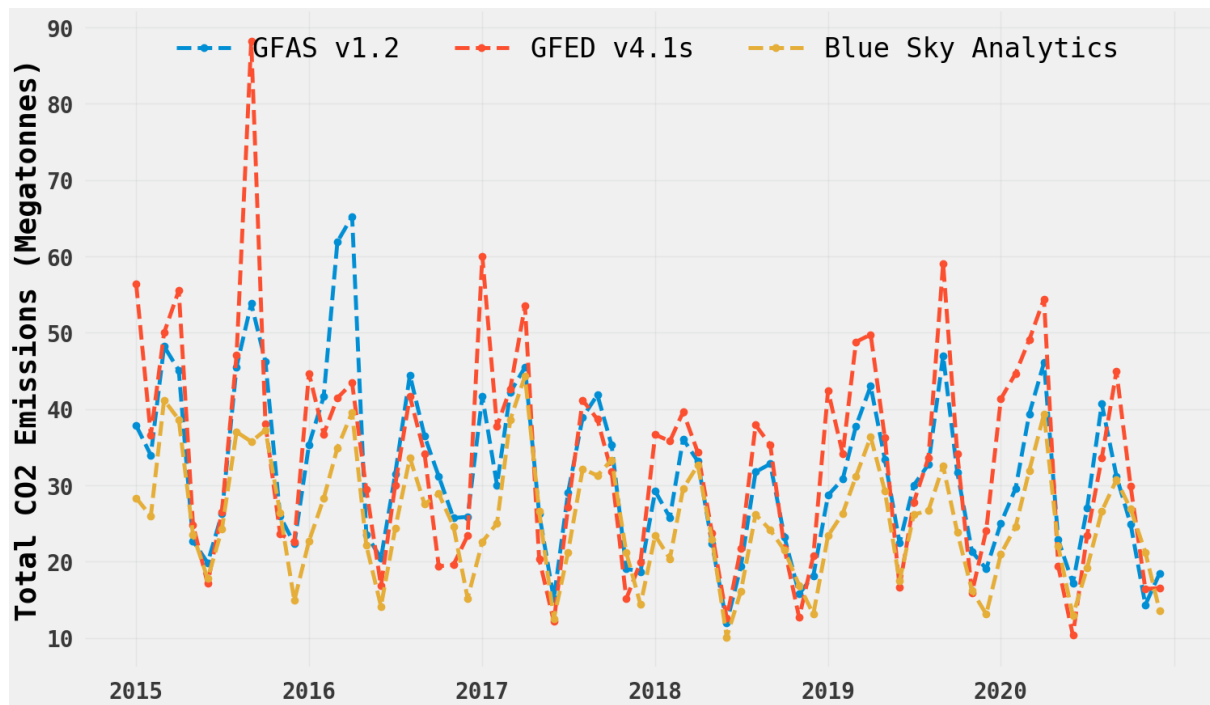
**Table 3** Parameter differences between Blue Sky Analytics GFAS v1.2, and GFED v4.1s.

Parameter	Blue Sky Analytics	GFAS	GFED
<i>Approach</i>	Top Down	Top Down	Bottom Up
<i>Fire detections (source and resolution)</i>	Suomi NPP VIIRS VNP14 (375m)	MOD14/MYD14 v5.0 & 6.0 (1km)	MCD64A1 v6.0 (Burnt Area Product) (500m)
<i>Number of fires</i>	SNPP is known to capture far a greater number of fires due to higher spatial resolution than MODIS active fire product	No	Y (Use small fire boost using statistical methods in GFED v4.1s)
<i>Output Resolution</i>	Aggregated at 0.25 degrees	0.125 degrees	0.25 degrees
<i>Fire detection thresholds</i>	50% confidence (for low confidence daytime fires) + excluding non-vegetation fires.	QA filters from MOD14/MYD14 data	QA filters from MCD64A1 data
<i>Land cover</i>	Copernicus CGLS 100m (2015-2019)	GFEDv4 dominant fire prone LULC	MCD12Q1 UMD Annual
<i>Emissions factors</i>	Andreae et al., (2019)	Andreae et al. (2001) and updates.	Akagi et al. (2011), with updates from M.O Andreae (2014),
<i>Combustion Coefficients or similar factors to get emissions</i>	Derived using relationships between TPM (AOD) and FRE (FRP) per land cover category	Derived using FRP and GFEDv4 DM conversion factor per land cover category	CASA biogeochemical model (Van der Werf, 2010)

### 3. Results and discussion

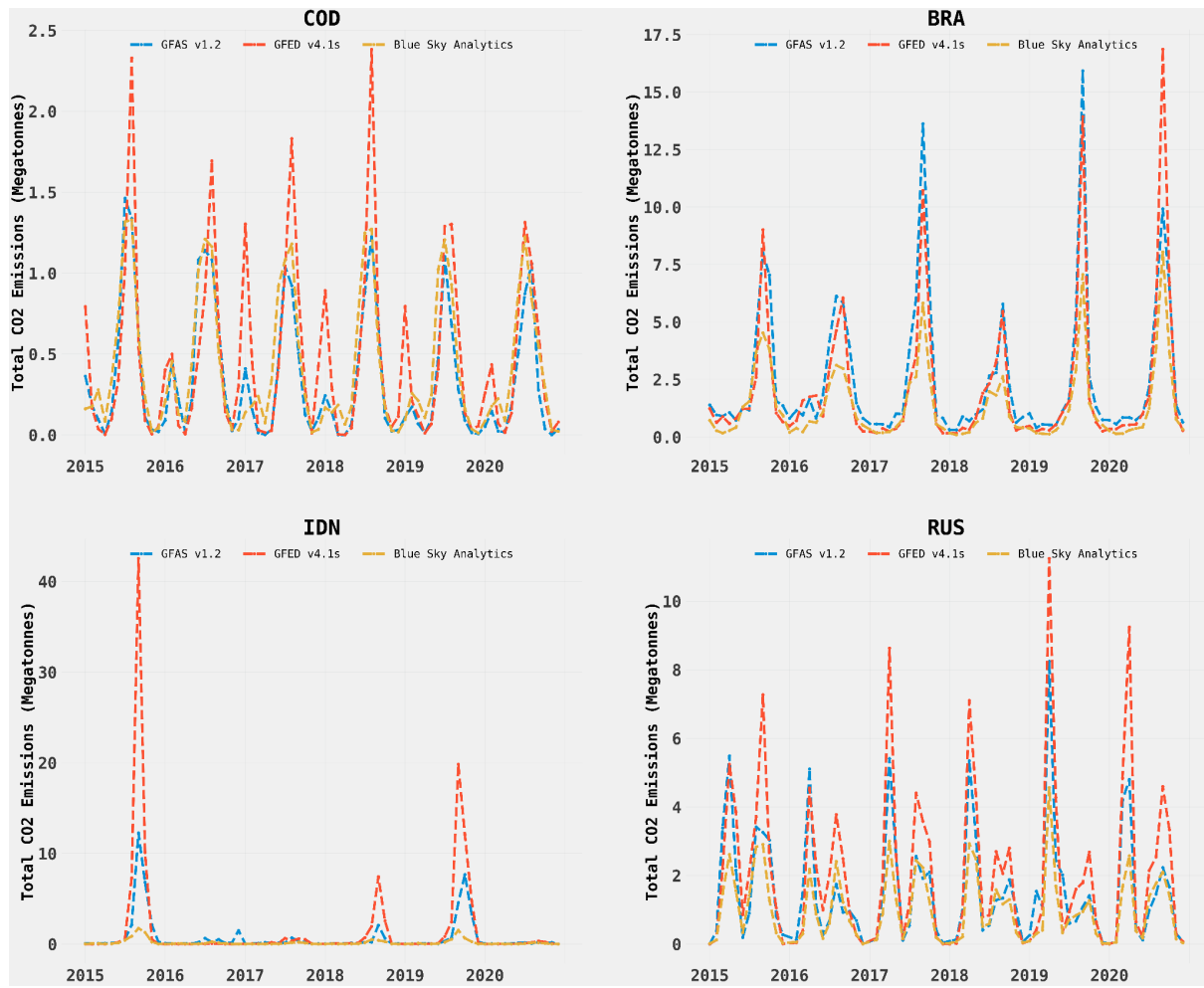
Although the methodology described in this document is used to generate emissions estimates for CO<sub>2</sub>, CH<sub>4</sub>, and N<sub>2</sub>O from global fire activity, in this section, we focus on the CO<sub>2</sub> estimates (the discussion on CH<sub>4</sub> and N<sub>2</sub>O is provided in the supplementary section, Figures 12 to 17). For comparison, all the emissions were aggregated on an annual scale for the period 2015 to 2020.

Figure 5 illustrates the comparison between BSA's estimates with GFAS and GFED for the total global CO<sub>2</sub> emissions from cropland fires from 2015 to 2020. Overall, BSA estimates follow a similar trend to GFAS and GFED. However, during the peak fire seasons, BSA's global estimates are relatively lower as compared to GFAS and GFED. As an example, BSA's estimates for 2015 are 38.6% and 21.8% less than those from GFED and GFAS, respectively. The BSA estimates for 2016 are also lower by 20.5% for GFED and 35% for GFAS. Overall, GFED estimates are relatively higher. Further, the comparison of BSA's estimates with GFED and GFAS was performed at the country level.



**Figure 5** Total global CO<sub>2</sub> emissions from cropland fires from 2015 to 2020- GFAS (blue line), GFED (orange line), and Blue Sky Analytics (yellow line). On the x-axis, January 1 is indicated as the year.

To further verify the estimates, we selected the top twelve countries that contributed to the emissions based on BSA's total emissions estimates from 2015 to 2020 (Figures 6, 7, and 8). The countries include the Democratic Republic of the Congo (COD), Brazil (BRA), Indonesia (IDN), Russia (RUS), Australia (AUS), Angola (AGO), United States of America (USA), Canada (CAN), India (IND), China (CHN), Myanmar (MMR), and Thailand (THA). This analysis at the country level indicates that for India and Australia, BSA's estimates are higher. For Angola and the Democratic Republic of the Congo, BSA's estimates are closer to GFAS. For Brazil, Indonesia, Russia, Canada, and Myanmar BSA's estimates are lower compared to the other two inventories.



**Figure 6** Comparison of monthly CO<sub>2</sub> emissions estimates from 2015 to 2020 for GFAS (blue line), GFED (orange line), and Blue Sky Analytics (yellow line) for the Democratic Republic of Congo (COD), Brazil (BRA), Indonesia (IDN), and Russia (RUS). Peaks indicate fire seasons, and dips indicate non-fire seasons.

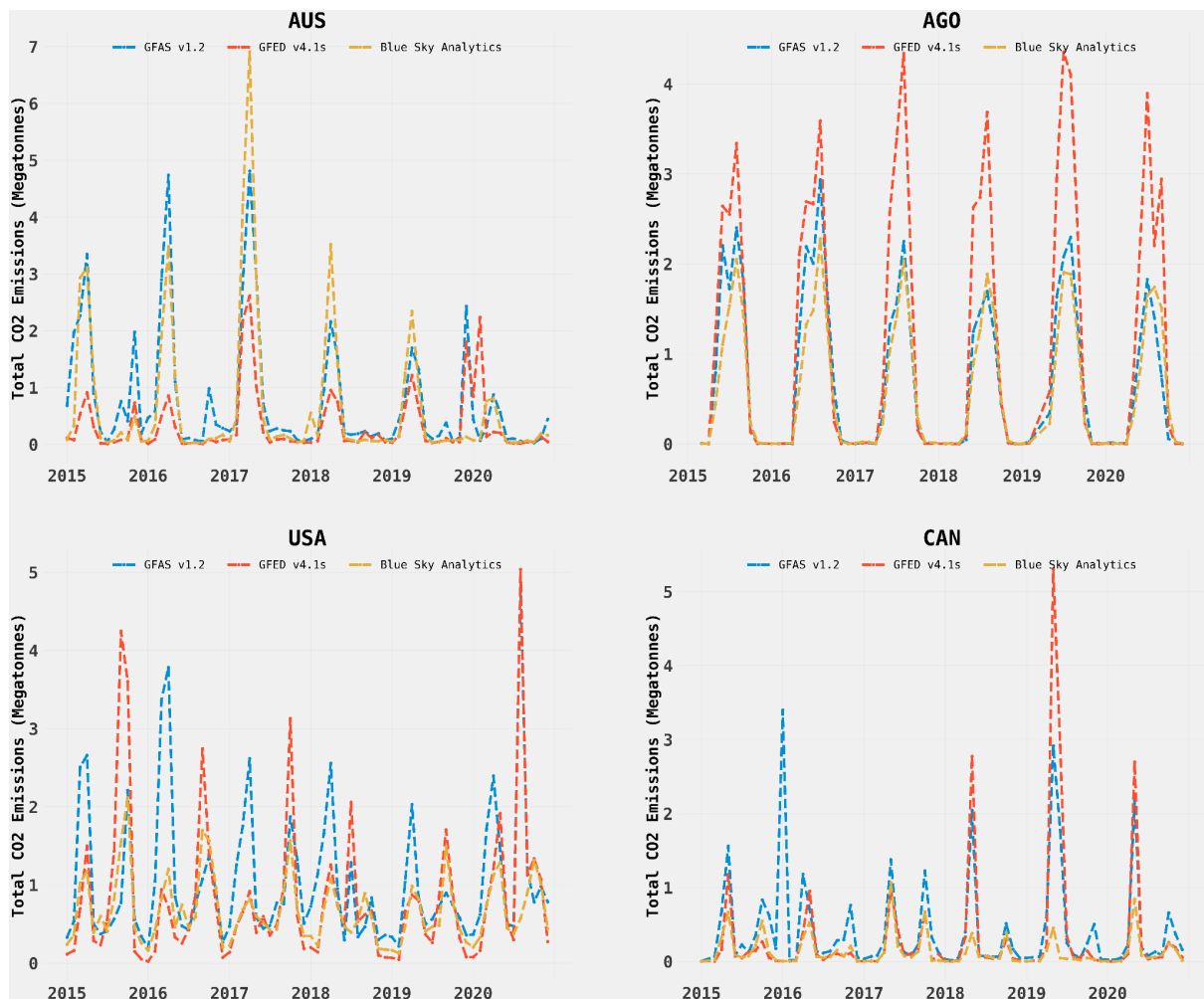


**Figure 7** Comparison of monthly CO<sub>2</sub> emissions estimates from 2015 to 2020 for GFAS (blue line), GFED (orange line), and Blue Sky Analytics (yellow line) for Australia (AUS), Angola (AGO), the United States of America (USA), and Canada (CAN). Peaks indicate fire seasons, and dips indicate non-fire seasons.

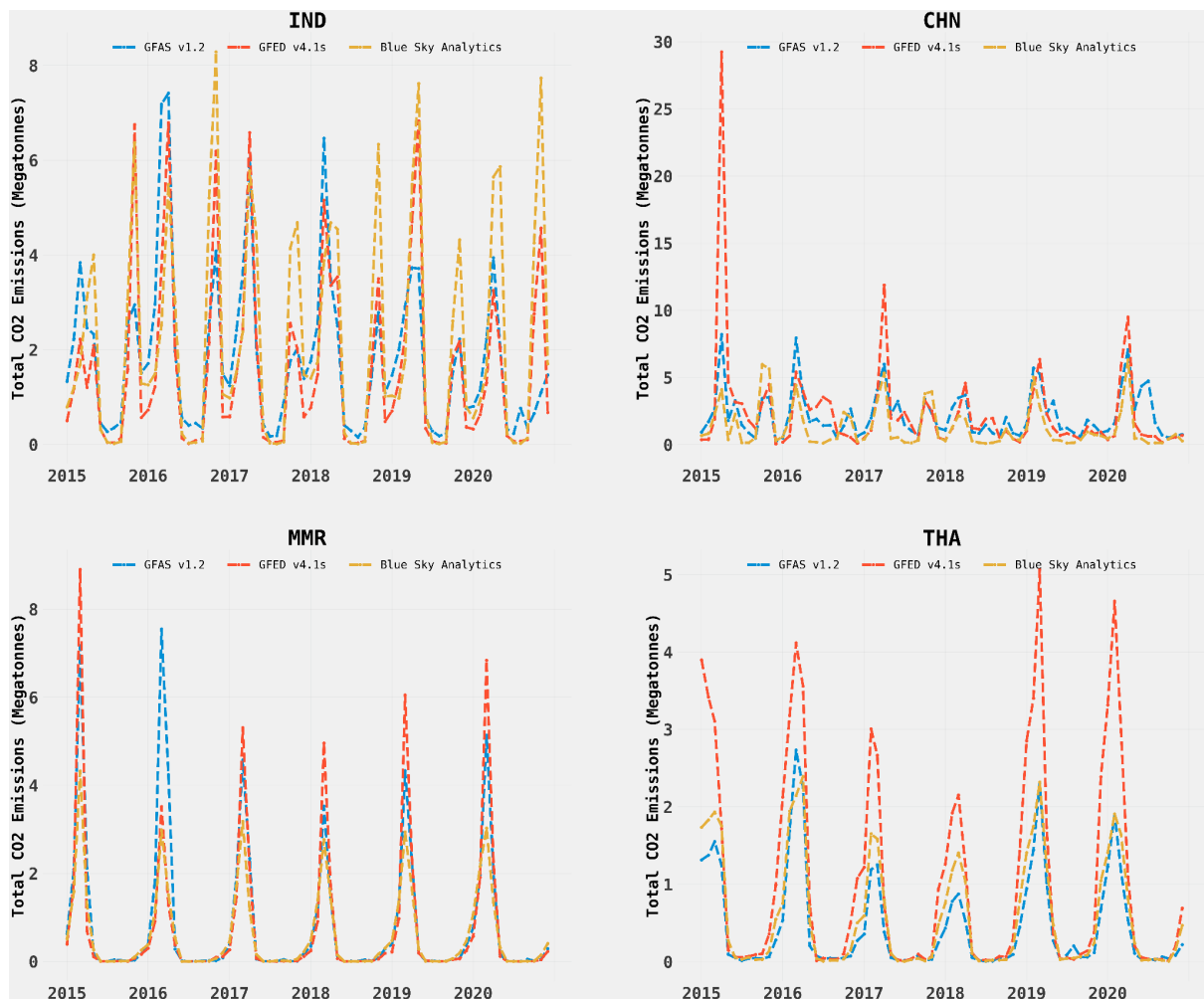
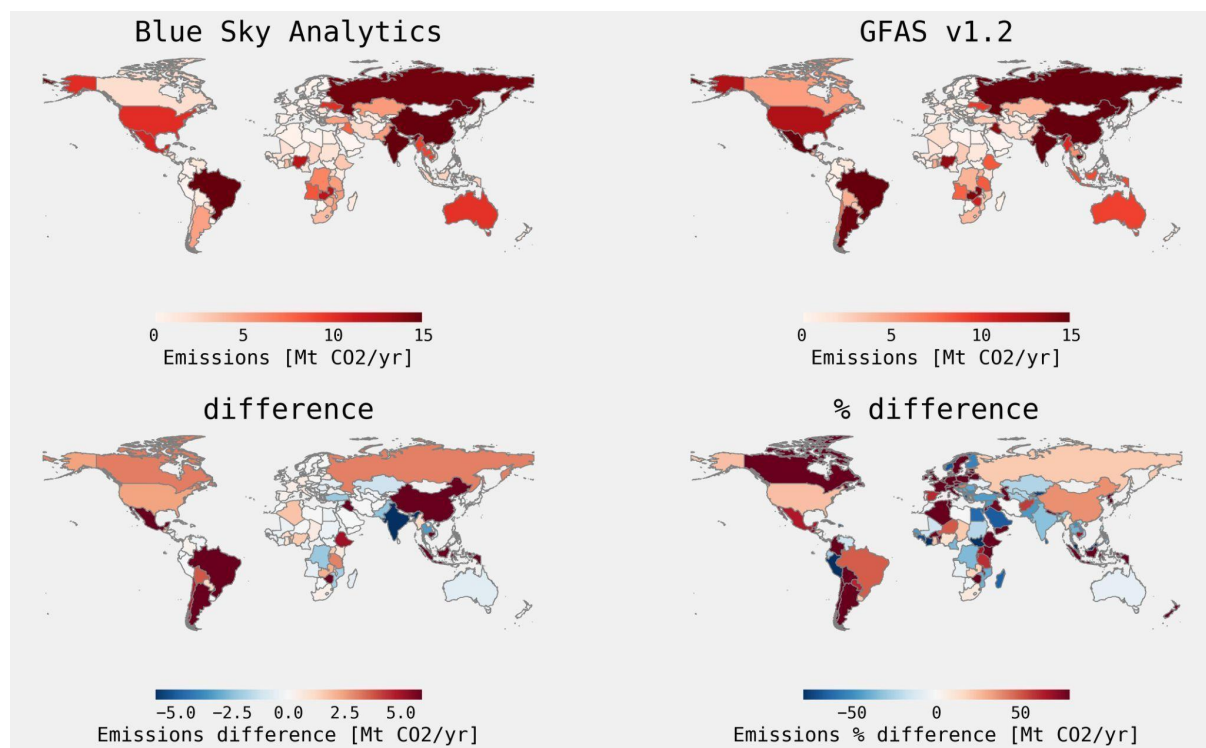


**Figure 8** Comparison of monthly CO<sub>2</sub> emissions estimates from 2015 to 2020 for GFAS (blue line), GFED (orange line), and Blue Sky Analytics (yellow line) for India (IND), China (CHN), Myanmar (MMR), and Thailand (THA). Peaks indicate fire seasons, and dips indicate non-fire seasons.

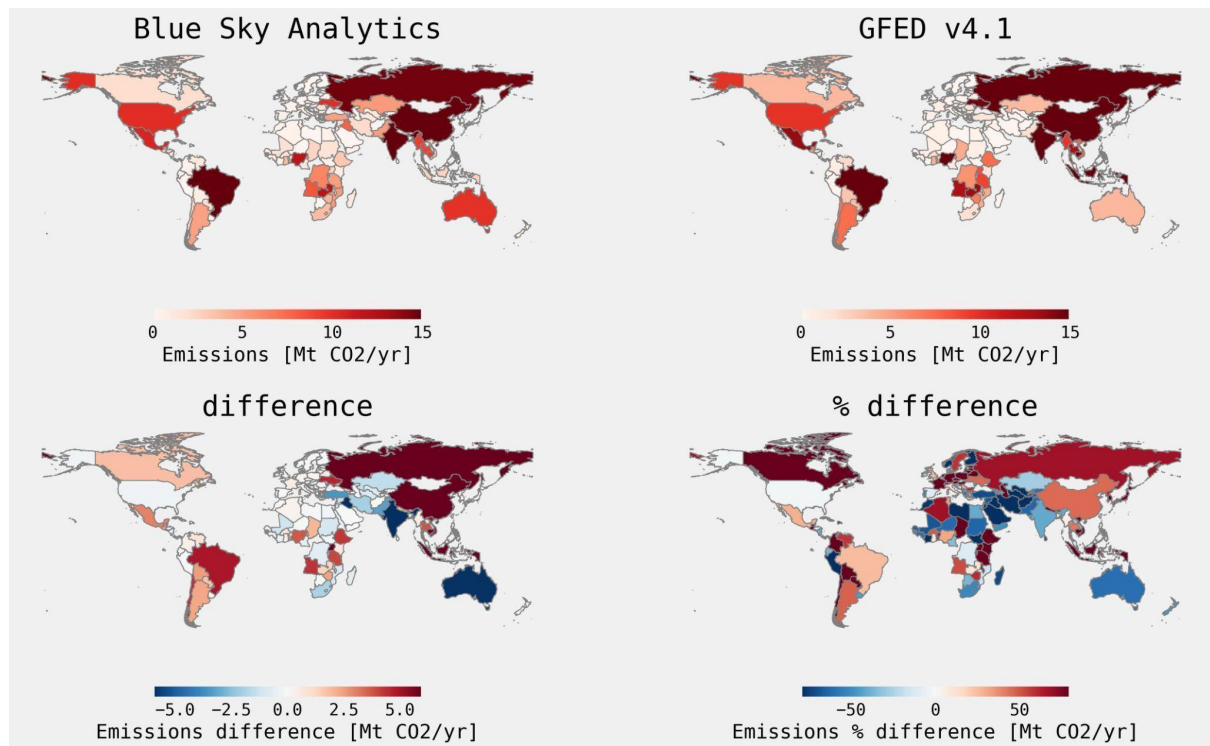
Figures 9 and 10 globally display emissions from this study with GFED and GFAS sources. The spatial distribution maps indicate that the top 5 major emitters are common in both BSA and GFAS 1.2, comprising - India, Brazil, China, Russia, and the USA, contributing almost 30% of the total CO<sub>2</sub> emissions (Figure 9). BSA's estimates are relatively lower as compared to GFAS for Brazil (35%), China (26%), the United States of America (14%), Russia (11%), and Myanmar (4%). Whereas BSA's estimates are relatively higher as compared to GFAS for India (37%), Angola (12%), Australia (14%), the Democratic Republic of Congo (39%), and Thailand (42%).

Figure 10 illustrates that the major emitters are common in BSA and GFED 1.2, comprising India, Brazil, China, Russia, USA, contributing approximately 30% of the total CO<sub>2</sub> emissions. BSA's estimates are relatively lower as compared to GFED for Angola (40%), Brazil (15%), China (34%), Russia (51%), and Thailand (31%). Whereas BSA's estimates are relatively higher as compared to GFED for Australia (AUS) (60%), the Democratic Republic

of Congo (COD) (17%), India (IND) (45%), Myanmar (MMR) (3%), and the United States of America (USA) (9%).



**Figure 9** Average global CO<sub>2</sub> emissions from fires from 2015 to 2020 - GFAS and Blue Sky Analytics. (Note: There are no emissions from the countries that are not plotted on the map.)



**Figure 10** Average global CO<sub>2</sub> emissions from cropland fires from 2015 to 2020 - GFED and Blue Sky Analytics. (Note: There are no emissions from the countries that are not plotted on the map.)

Comparing BSA's estimates against GFAS v1.2 (Figure 11a) at a monthly frequency result in the mean absolute error (MAE) of 4.5 MtCO<sub>2</sub>/month, the mean absolute percentage error (MAPE) of 0.14, and r<sup>2</sup> score of 0.64. By comparing BSA's estimates with GFED v4.1 (Figure 11b) at a monthly frequency, the MAE was 7.1 MtCO<sub>2</sub>/month, the MAPE was 0.21, and the r<sup>2</sup> score was 0.46.

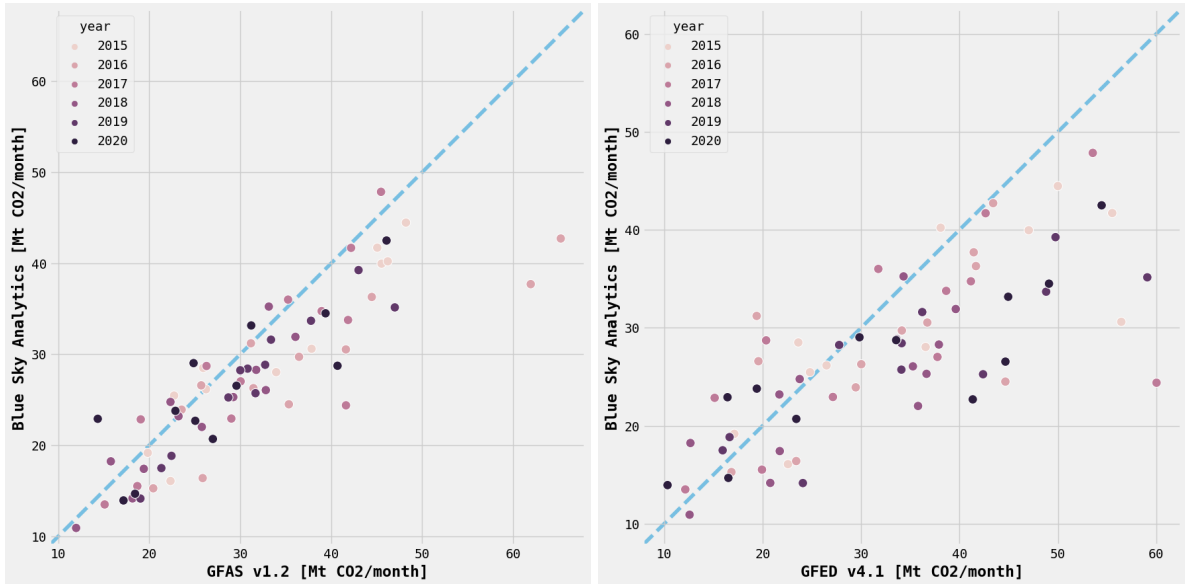


**Figure 11** Comparison of a) BSA and GFAS monthly average emissions (Gtonnes CO<sub>2</sub>/yr), b) BSA and GFED monthly average emissions (Gtonnes CO<sub>2</sub>/yr). The line of equality is shown in blue.

#### 4. Conclusion and future scope

This document describes the methodology for the global dataset of estimated GHG emissions from cropland biomass burning. It builds upon existing lines of research, particularly those based on a top-down approach to GHG emissions. It used VIIRS over MODIS to capture fire events which significantly helped estimate emissions from small fires, which could be significant in agricultural-majority nations. Even though we derived combustion coefficients ( $C_e$ ) specific to cropland in the current approach, differences in emissions estimation exist across regions when compared with other global inventories. Future versions of the study would investigate the reasons for these regional differences.

The estimated emissions depend on the number of active fire incidents captured from the area of interest at the time of the satellite pass. The possibility exists that many fires remain undetected, resulting in an underestimation of emissions. There are several reasons we know for the missing fires and the underestimation of emissions:

- **Small fires:** The fire's size (less than 375 m x 375 m) is too small to be detected by the satellite sensor.
- **Fires with short duration:** The satellite data capture active fires every 24 hours. Agriculture fires last just a short period (lasting less than 24 hours), unlike forest fires or wildfires. When satellites pass over such short-lived fires, they become cooler and undetected.
- **Haziness, cloud cover:** Smoke or thick clouds also obscure fires.

As part of this version, we do not consider fires that are missed due to cloud coverage, fires with short duration and smaller size, which could explain the slightly lower overall emissions compared to other inventories.

The current approach relies on polar satellites to capture the fires. Even though polar satellite observations are near real-time, they only produce two observations per location, which might not be sufficient to characterize fire activity variation throughout the day fully. The future goal is to integrate the fire observations from geostationary satellites (for example, SEVIRI, Geostationary Operational Environmental Satellite (GOES) series, and HIMAWARI) to reduce the errors caused by the low time resolution of polar satellites. Future versions of emissions estimations will address these limitations.

## Supplementary materials

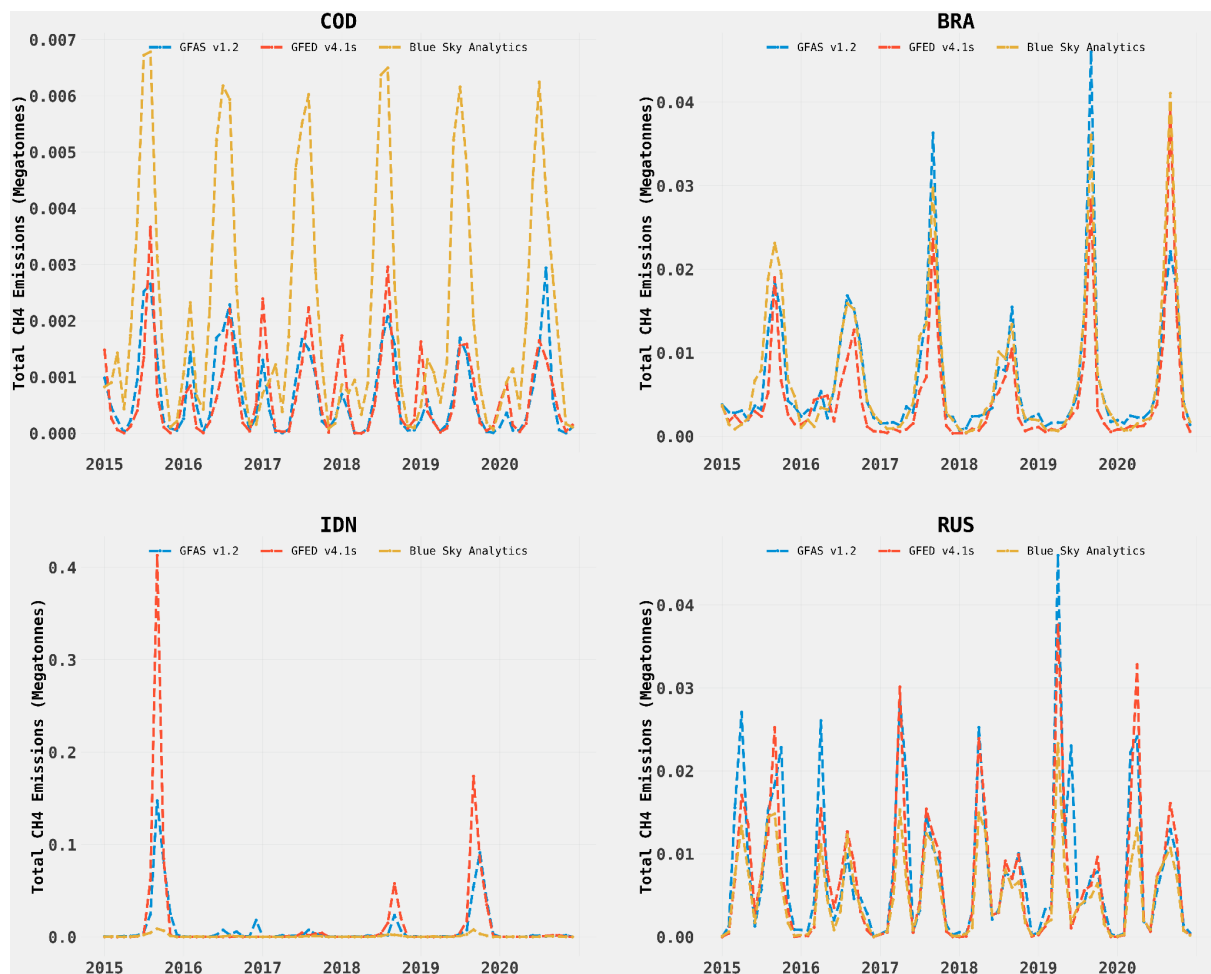


**Figure 12** Comparison of monthly  $\text{CH}_4$  emissions estimates from 2015 to 2020 for GFAS (blue line), GFED (orange line), and Blue Sky Analytics (yellow line) for the Democratic Republic of Congo (COD), Brazil (BRA), Indonesia (IDN) and Russia (RUS). Peaks indicate fire seasons, and dips indicate non-fire seasons.

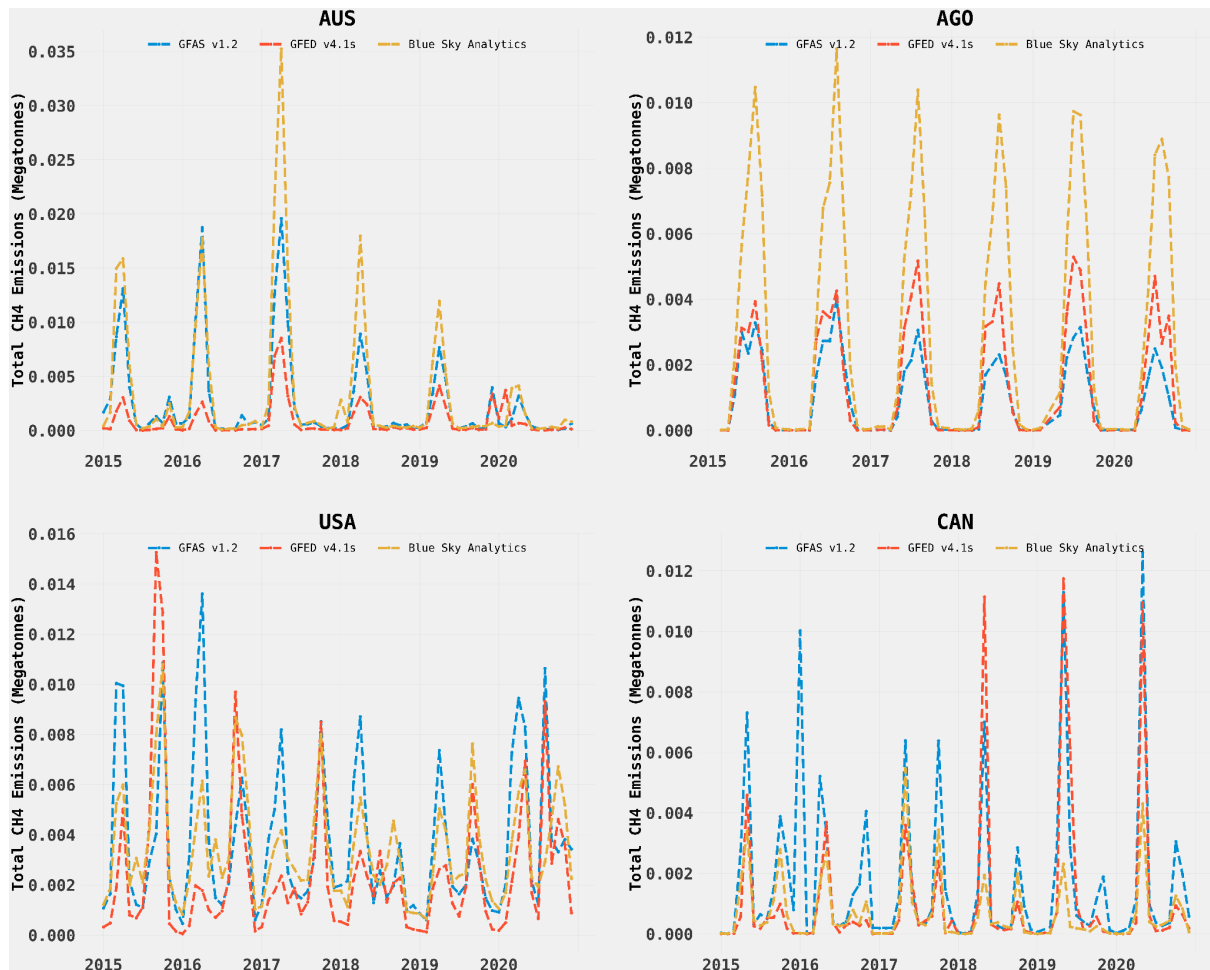


**Figure 13** Comparison of monthly CH<sub>4</sub> emissions estimates from 2015 to 2020 for GFAS (blue line), GFED (orange line), and Blue Sky Analytics (yellow line) for Australia (AUS), Angola (AGO), the United States of America (USA) and Canada (CAN). Peaks indicate fire seasons, and dips indicate non-fire seasons.

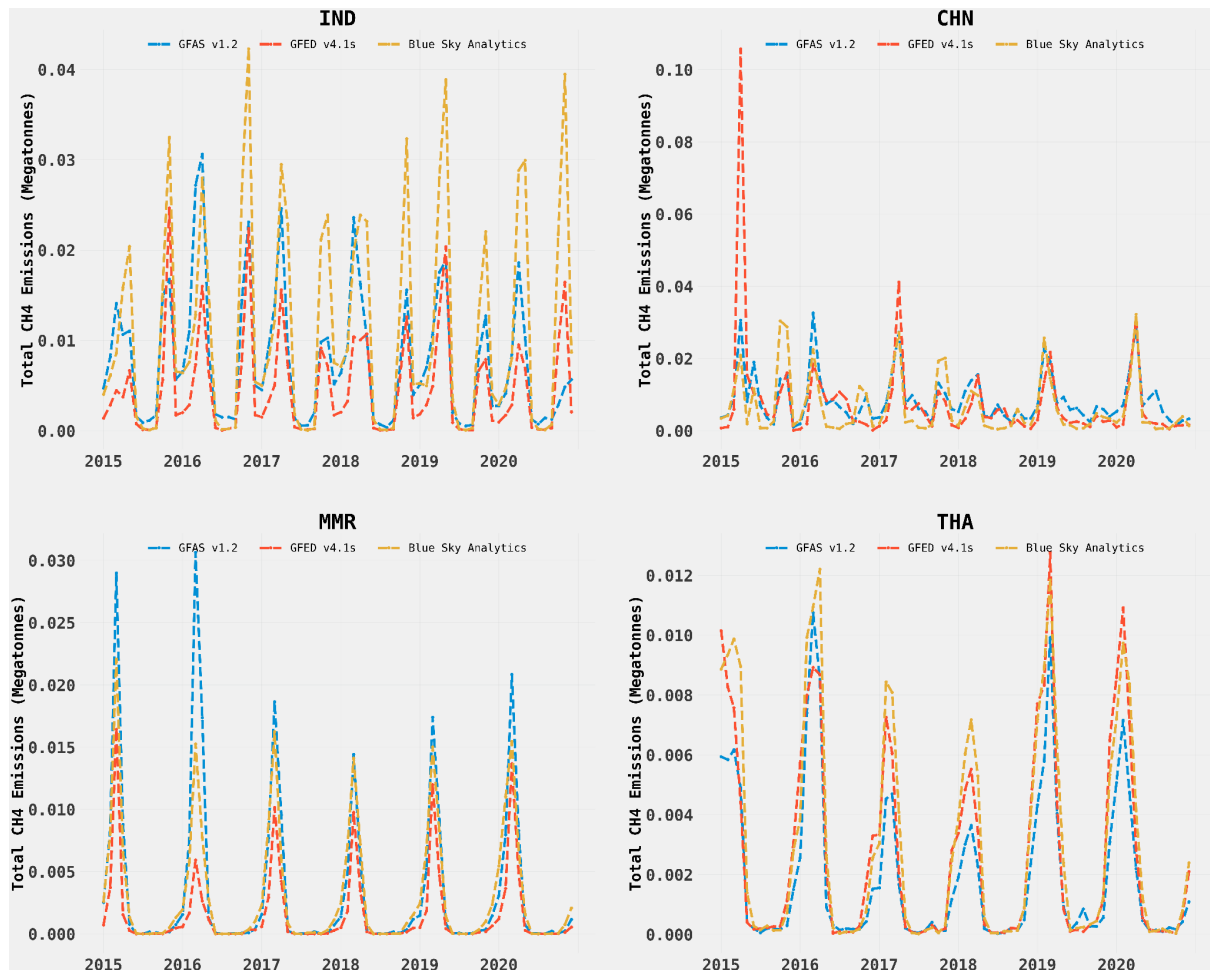


**Figure 14** Comparison of monthly CO<sub>2</sub> emissions estimates from 2015 to 2020 for GFAS (blue line), GFED (orange line), and Blue Sky Analytics (yellow line) for India (IND), China (CHN), Myanmar (MMR) and Thailand (THA). Peaks indicate fire seasons, and dips indicate non-fire seasons.

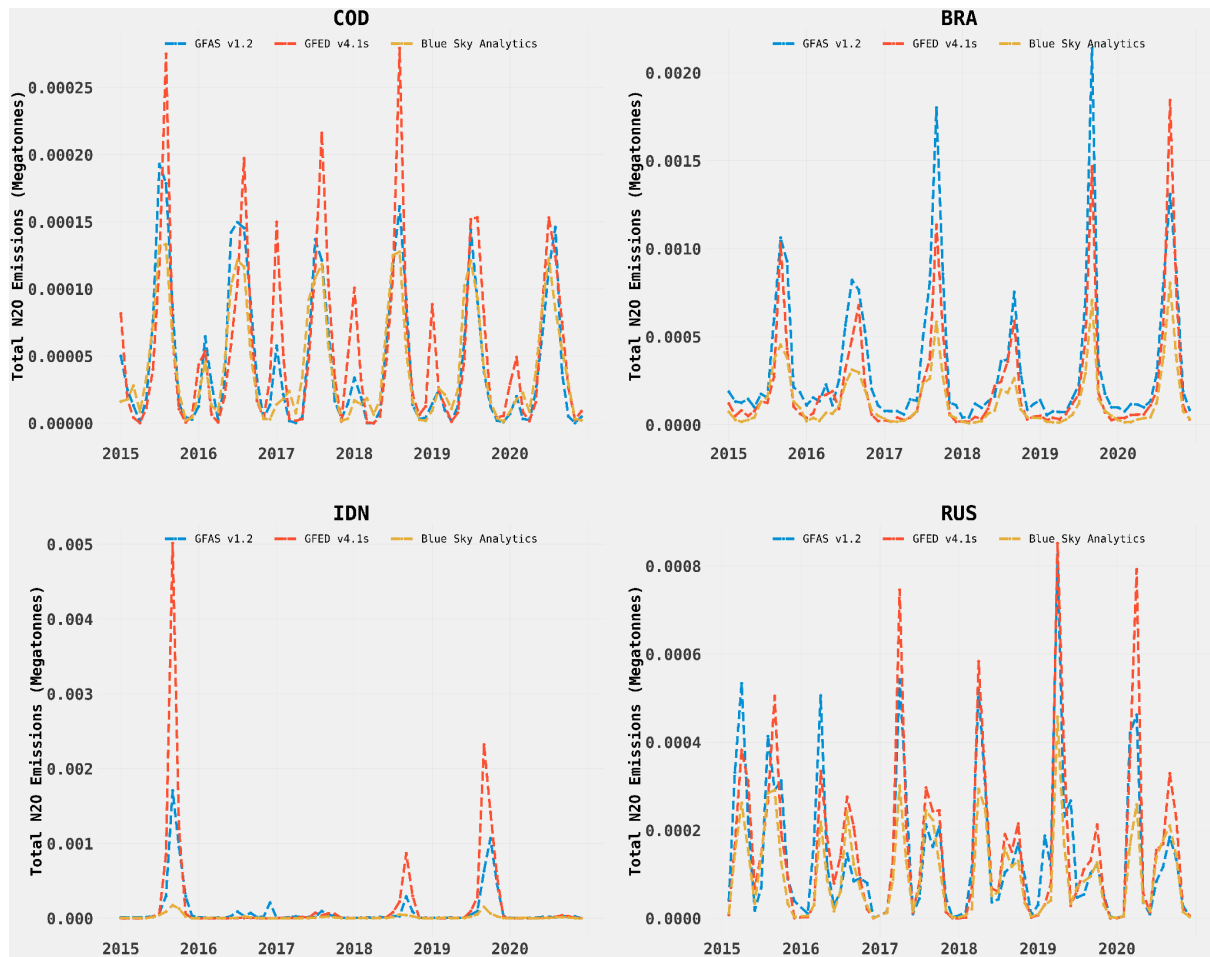


**Figure 15** Comparison of monthly N<sub>2</sub>O emissions estimates from 2015 to 2020 for GFAS (blue line), GFED (orange line), and Blue Sky Analytics (yellow line) for the Democratic Republic of Congo (COD), Brazil (BRA), Indonesia (IDN) and Russia (RUS). Peaks indicate fire seasons, and dips indicate non-fire seasons.

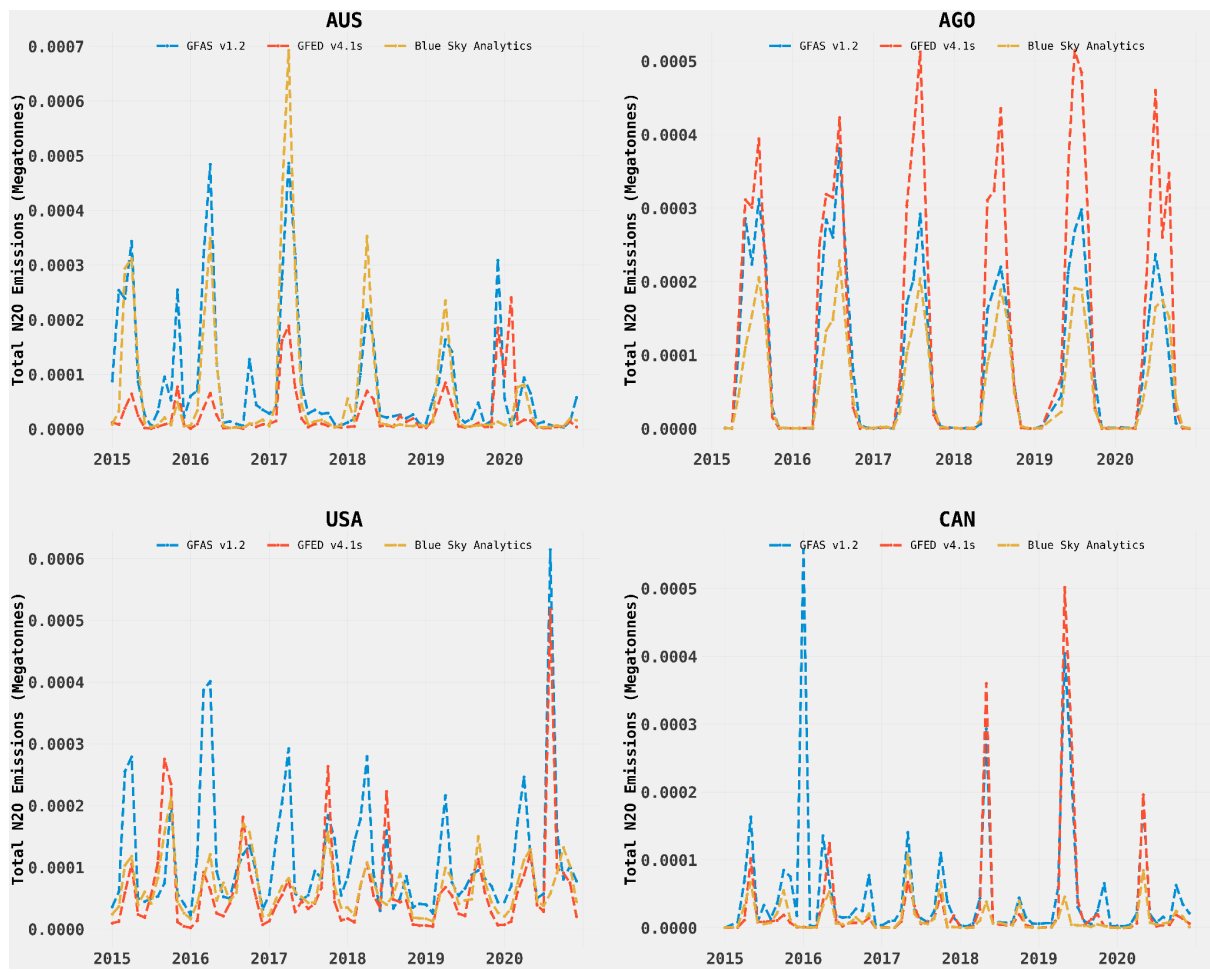


**Figure 16** Comparison of monthly N<sub>2</sub>O emissions estimates from 2015 to 2020 for GFAS (blue line), GFED (orange line), and Blue Sky Analytics (yellow line) for Australia (AUS), Angola (AGO), the United States of America (USA) and Canada (CAN). Peaks indicate fire seasons, and dips indicate non-fire seasons.

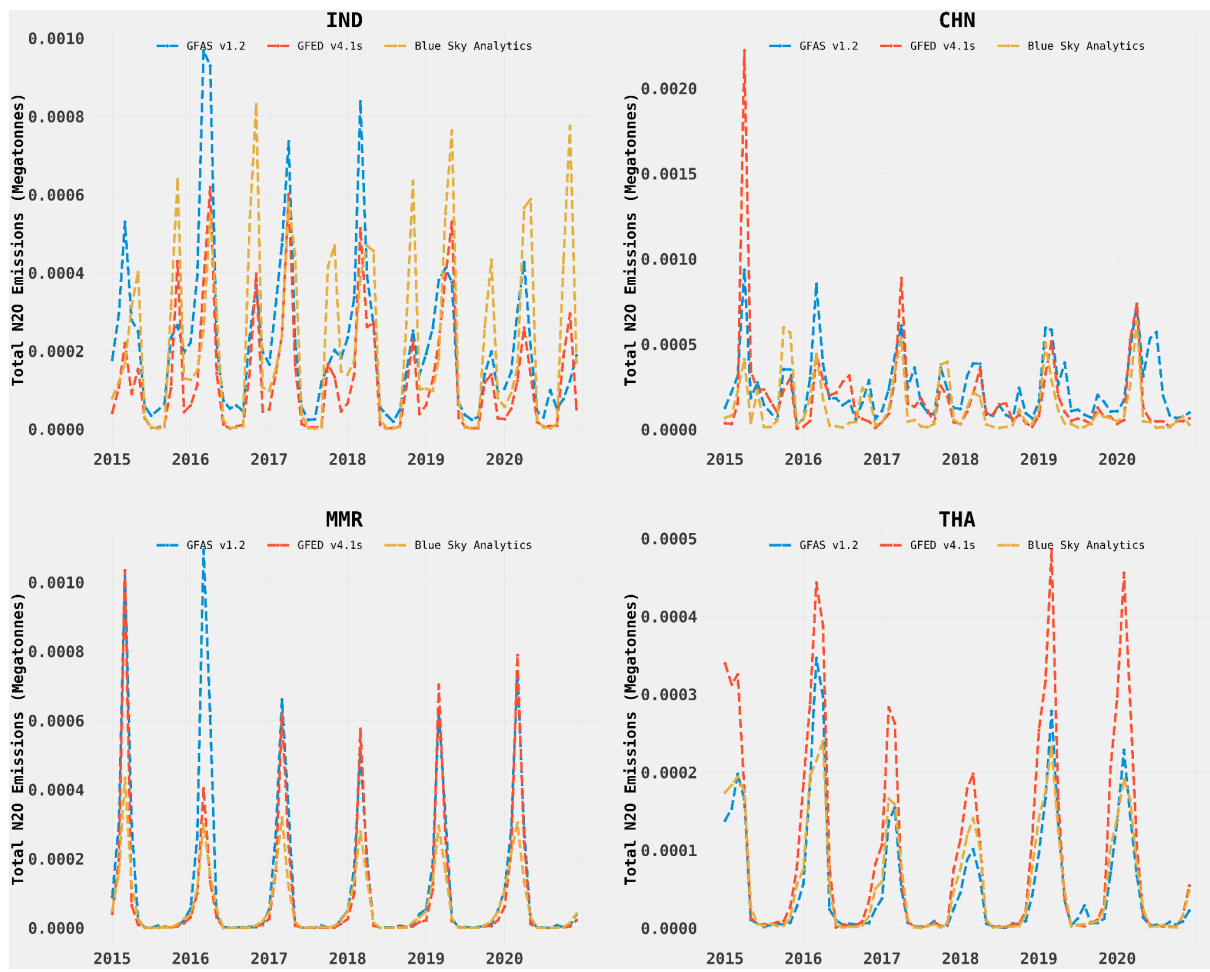


**Figure 17** Comparison of monthly N<sub>2</sub>O emissions estimates from 2015 to 2020 for GFAS (blue line), GFED (orange line), and Blue Sky Analytics (yellow line) for India (IND), China (CHN), Myanmar (MMR) and Thailand (THA). Peaks indicate fire seasons, and dips indicate non-fire seasons.

## References

1. Andela, N., Kaiser, J.W., van der Werf, G.R., Wooster, M.J., 2015. New fire diurnal cycle characterizations to improve fire radiative energy assessments made from MODIS observations. *Atmospheric Chem. Phys.* 15, 8831–8846. <https://doi.org/10.5194/acp-15-8831-2015>
2. Andreae, M.O., 2019. Emission of trace gases and aerosols from biomass burning – an updated assessment. *Atmospheric Chem. Phys.* 19, 8523–8546. <https://doi.org/10.5194/acp-19-8523-2019>
3. Andreae, M.O., Merlet, P., 2001. Emission of trace gases and aerosols from biomass burning. *Glob. Biogeochem. Cycles* 15, 955–966. <https://doi.org/10.1029/2000GB001382>
4. Buchhorn, M., Smets, B., Bertels, L., Roo, B.D., Lesiv, M., Tsendbazar, N.-E., Herold, M., Fritz, S., 2020. Copernicus Global Land Service: Land Cover 100m: collection 3: epoch 2019: Globe. <https://doi.org/10.5281/ZENODO.3939050>
5. Forster, P., Storelvmo, T., Armour, K., Collins, W., Dufresne, J.-L., Frame, D., Lunt,

- D.J., Mauritsen, T., Palmer, M.D., Watanabe, Manabu, Wild, M., Zhang, H., 2021. Chapter 7: The Earth's Energy Budget, Climate Feedbacks and Climate Sensitivity, in Climate Change 2021: The Physical Science Basis. Contribution of Working Group I to the Sixth Assessment Report of the Intergovernmental Panel on Climate Change. Cambridge University Press, Cambridge, United Kingdom and New York, NY, USA.
6. Freeborn, P.H., Wooster, M.J., Hao, W.M., Ryan, C.A., Nordgren, B.L., Baker, S.P., Ichoku, C., 2008. Relationships between energy release, fuel mass loss, and trace gas and aerosol emissions during laboratory biomass fires. *J. Geophys. Res.* 113, D01301. <https://doi.org/10.1029/2007JD008679>
  7. Giglio Louis, Justice Christopher, 2015. MOD14A1 MODIS/Terra Thermal Anomalies/Fire Daily L3 Global 1km SIN Grid V006. <https://doi.org/10.5067/MODIS/MOD14A1.006>
  8. Hudak, A.T., Dickinson, M.B., Bright, B.C., Kremens, R.L., Loudermilk, E.L., O'Brien, J.J., Hornsby, B.S., Ottmar, R.D., 2016. Measurements relating fire radiative energy density and surface fuel consumption – RxCADRE 2011 and 2012. *Int. J. Wildland Fire* 25, 25. <https://doi.org/10.1071/WF14159>
  9. Ichoku, C., Ellison, L., 2014. Global top-down smoke-aerosol emissions estimation using satellite fire radiative power measurements. *Atmospheric Chem. Phys.* 14, 6643–6667. <https://doi.org/10.5194/acp-14-6643-2014>
  10. Ichoku, C., Kaufman, Y.J., 2005. A method to derive smoke emission rates from MODIS fire radiative energy measurements. *IEEE Trans. Geosci. Remote Sens.* 43, 2636–2649.
  11. Jacobson, M.Z., 2014. Effects of biomass burning on climate, accounting for heat and moisture fluxes, black and brown carbon, and cloud absorption effects: Effects of biomass burning on climate. *J. Geophys. Res. Atmospheres* 119, 8980–9002. <https://doi.org/10.1002/2014JD021861>
  12. Johnston, J.M., Jackson, N., McFayden, C., Ngo Phong, L., Lawrence, B., Davignon, D., Wooster, M.J., van Mierlo, H., Thompson, D.K., Cantin, A.S., Johnston, D., Johnston, L.M., Sloane, M., Ramos, R., Lynham, T.J., 2020. Development of the User Requirements for the Canadian WildFireSat Satellite Mission. *Sensors* 20, 5081. <https://doi.org/10.3390/s20185081>
  13. Kaiser, J.W., Heil, A., Andreae, M.O., Benedetti, A., Chubarova, N., Jones, L., Morcrette, J.-J., Razinger, M., Schultz, M.G., Suttie, M., van der Werf, G.R., 2012. Biomass burning emissions estimated with a global fire assimilation system based on observed fire radiative power. *Biogeosciences* 9, 527–554. <https://doi.org/10.5194/bg-9-527-2012>
  14. Kasischke, E.S., Loboda, T., Giglio, L., French, N.H.F., Hoy, E.E., de Jong, B., Riano, D., 2011. Quantifying burned area for North American forests: Implications for direct reduction of carbon stocks. *J. Geophys. Res.* 116, G04003. <https://doi.org/10.1029/2011JG001707>
  15. Korontzi, S., McCarty, J., Loboda, T., Kumar, S., Justice, C., 2006. Global distribution of agricultural fires in croplands from 3 years of Moderate Resolution Imaging Spectroradiometer (MODIS) data: Global Distribution Of Agricultural Fire. *Glob. Biogeochem. Cycles* 20, <https://doi.org/10.1029/2005GB002529>

16. Lyapustin, A., Wang, Y., Korkin, S., Huang, D., 2018. MODIS Collection 6 MAIAC algorithm. *Atmospheric Meas. Tech.* 11, 5741–5765. <https://doi.org/10.5194/amt-11-5741-2018>
17. Lyapustin, A., Wang, Y., Laszlo, I., Kahn, R., Korkin, S., Remer, L., Levy, R., Reid, J.S., 2011. Multiangle implementation of atmospheric correction (MAIAC): 2. Aerosol algorithm. *J. Geophys. Res.* 116, D03211. <https://doi.org/10.1029/2010JD014986>
18. Mota, B., Wooster, M.J., 2018. A new top-down approach for directly estimating biomass burning emissions and fuel consumption rates and totals from geostationary satellite fire radiative power (FRP). *Remote Sens. Environ.* 206, 45–62. <https://doi.org/10.1016/j.rse.2017.12.016>
19. Ramo, R., Roteta, E., Bistinas, I., van Wees, D., Bastarrika, A., Chuvieco, E., van der Werf, G.R., 2021. African burned area and fire carbon emissions are strongly impacted by small fires undetected by coarse resolution satellite data. *Proc. Natl. Acad. Sci.* 118, e2011160118. <https://doi.org/10.1073/pnas.2011160118>
20. Randerson, J.T., Van der Werf, G.R., Giglio, L., Collatz, G.J., Kasibhatla, P.S., 2017. Global Fire Emissions Database, Version 4.1 (GFEDv4) 1925.7122549999906 MB. <https://doi.org/10.3334/ORNLDaac/1293>
21. Seiler, W., Crutzen, P.J., 1980. Estimates of gross and net fluxes of carbon between the biosphere and the atmosphere from biomass burning. *Clim. Change* 2, 207–247. <https://doi.org/10.1007/BF00137988>
22. U.S. Environmental Protection Agency, 2021. Inventory of U.S. greenhouse gas emissions and sinks: 1990 – 2019. Available at: <https://www.epa.gov/sites/default/files/2021-04/documents/us-ghg-inventory-2021-main-text.pdf>
23. Van der Werf, G.R., Randerson, J.T., Giglio, L., Collatz, G.J., Kasibhatla, P.S., Arellano, A.F., 2006. Interannual variability in global biomass burning emissions from 1997 to 2004. *Atmospheric Chem. Phys.* 6, 3423–3441. <https://doi.org/10.5194/acp-6-3423-2006>
24. Van der Werf, G.R., Randerson, J.T., Giglio, L., Collatz, G.J., Mu, M., Kasibhatla, P.S., Morton, D.C., DeFries, R.S., Jin, Y., van Leeuwen, T.T., 2010. Global fire emissions and the contribution of deforestation, savanna, forest, agricultural, and peat fires (1997–2009). *Atmospheric Chem. Phys.* 10, 11707–11735. <https://doi.org/10.5194/acp-10-11707-2010>
25. Van der Werf, G.R., Randerson, J.T., Giglio, L., van Leeuwen, T.T., Chen, Y., Rogers, B.M., Mu, M., van Marle, M.J.E., Morton, D.C., Collatz, G.J., Yokelson, R.J., Kasibhatla, P.S., 2017. Global fire emissions estimates during 1997–2016. *Earth Syst. Sci. Data* 9, 697–720. <https://doi.org/10.5194/essd-9-697-2017>
26. Vermote, E., Ellicott, E., Dubovik, O., Lapyonok, T., Chin, M., Giglio, L., Roberts, G.J., 2009. An approach to estimate global biomass burning emissions of organic and black carbon from MODIS fire radiative power. *J. Geophys. Res.* 114, D18205. <https://doi.org/10.1029/2008JD011188>
27. Wooster, M.J., Roberts, G., Perry, G.L.W., Kaufman, Y.J., 2005. Retrieval of biomass combustion rates and totals from fire radiative power observations: FRP derivation

- and calibration relationships between biomass consumption and fire radiative energy release. *J. Geophys. Res.* 110, D24311. <https://doi.org/10.1029/2005JD006318>
28. Xun, L., Lu, H., Qian, C., Zhang, Y., Lyu, S., Li, X., 2021. Analysis of Aerosol Optical Depth from Sun Photometer at Shouxian, China. *Atmosphere* 12, 1226. <https://doi.org/10.3390/atmos12091226>